Nanoscale

Accepted Manuscript

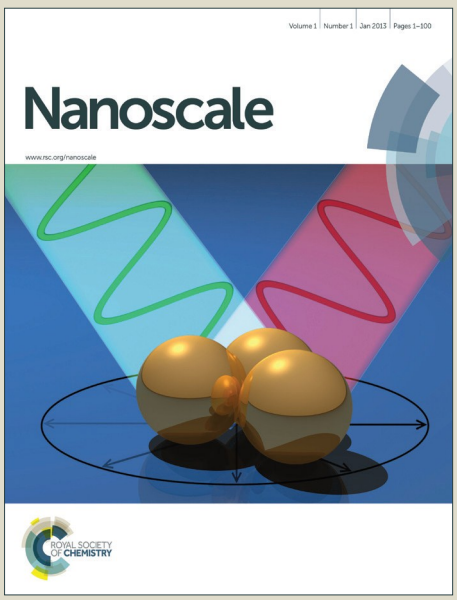

ROYAL SOCIETY OF CHEMISTRY

www.rsc.org/nanoscale

Journal Name

RSCPublishing

ARTICLE

Megranate-Like Nanoreactor with Multiple Cores and an Acidic Mesoporous Shell for a Cascade Reaction

Cite this: DOI: 10.1039/xoxxoooooox

Received ooth January 2012,
Accepted ooth January 2012

DOI: 10.1039/xoxxoooooox

www.rsc.org/

Xue Wang, Buyuan Guan, Yapeng He, Dong An, Ye Zhang, Yu Cao, Xiang Li, Yunling Liu and Qisheng Huo*

Different from simple yolk-shell nanoparticle, megranate-like nanoparticle possesses a unique structure that is composed of multiple cores and shell. Megranate-like nanoparticles can combine the properties of each component and be used as nanoreactors. This contribution describes the preparation of bifunctional megranate-like nanoreactors consisting of multiple metal cores and thoil modified mesoporous SiO_2 shells. The different metal nanoparticles (Pd, Pt, Au) can be incorporated into the structure as cores, and thoil group in shells can be oxidized to acidic -SO_3H. The megranate-like nanoparticles show good bifunctional catalytic properties and recyclability in a cascade catalytic reaction for desired benzimidazole derivative. And the individual component of the megranate-like nanoparticles also shows good catalytic activities in the hydrogenation reduction of nitro-aromatics and the deprotection of benzaldehyde dimethyl acetal reaction.

Introduction

Recently, so-called yolk-shell nanostructures or rattle-type nanomaterials with a void space between the core and the shell of the material have been paid much attention as a new member of hollow nanoarchitectures.[1-4] Owing to their unusual properties of low density, high surface areas, and interstitial hollow spaces, they have been widely applied in many important research fields,[5-13] including catalysis,[6, 7, 13] and nanoreactors.[8, 9] The catalytic activities of yolk-shell nanoparticles have been chalked up to the freely movable core catalysts, and the protective shell.[11, 12] Since the movable cores can afford exposed active sites, the shell can not only allow fast diffusion of reactants and product, but also protect the cores and keep the cores stable even under harsh conditions.[14-16] Compared with simple yolk-shell nanoparticles, megranate-like nanoparticles own multiple cores.[17-20] They can afford more exposed active sites and show better catalytic activities.[21-24] Therefore, megranate-like nanoparticles with many catalytically active cores have presented promising applications in catalytic field as nanoreactors.

For the synthesis of yolk-shell nanostructures with desired components, many synthetic methods have been developed, including the ship-in-bottle approach,[25] selective etching approaches,[26, 27] bottom-up or soft templating approaches,[28, 29] template-free approaches,[30] Ostwald ripening[31] or galvanic replacement processes,[32] and methods based on the Kirkendall effect.[2] Applying them, various yolk–shell nanoparticles with different chemical compositions, including Pt@CeO_2,[22] Au@SiO_2,[24] Fe_3O_4@SiO_2[26] and polymer@polymer[27] have been synthesized.

However, great efforts have been devoted to synthesize desired catalytically active core, few studies focus on the utilizing catalytically active shells,[33-35] and the permeable shell is only responsible for preventing aggregation from the core and protecting the core, so few yolk-shell nanoreactors previously reported were applied in multi-step catalytic reactions.[11, 36-38] With the using of a multifunctional megranate-like nanoparticle as catalyst, the multistep reactions can be conducted in a one-pot reaction. It reduces the steps of purification and separation, the amount of reagents and wastes,[39] it also reduces the cost of getting final products, so these hybrid materials will have potential applications in catalytic field.[33, 40-42] Compared with single solid catalysts, multifunctional megranate-like nanoparticles can also combine different components together.[17, 19] It may reduce the interaction between different components comparing with simple mixing. Therefore, the work of designing and synthesizing multifunctional megranate-like nanoreactor with multiple cores and catalytically active shell, applicating megranate-like nanoreactor in cascade reactions would be very meaningful.

Herein, using simple yolk-shell nanoparticles as substrates, we synthesize multifunctional megranate-like nanoparticles consisting of multiple metal nanoparticles as the cores, and mesoporous SiO_2 shells functionalized with 3-mercaptopropyl groups. We can incorporate different metal nanoparticles (Pd, Pt, Au) into the hollow structure. We can also process the shell through oxidizing of the SH groups making it possessing acidity (-SO_3H). We prove the catalytic activities of individual group and the whole megranate-like structures as nanoreactors. The megranate-like structures as bifunctional catalysts show good activities in a cascade catalytic reaction for desired benzimidazole derivative. And Pd nanoparticles show good catalytic activities and stability in the hydrogenation reduction of nitro-aromatics. The shells also show good acidity in the deprotection of the benzaldehyde dimethyl acetal reaction.

Experimental

Chemicals

TEOS was obtained from Sigma-Aldrich. 3-aminopropyltriethoxysilane (APTES), *N*-[3-(trimethoxysilyl) propyl] ethylenediamine (TSD), (3-mercaptopropyl) trimethoxysilane (MPTMS), benzaldehyde dimethyl acetal, benzaldehyde, 4-nitrobenzaldehyde, 1, 2-phenylenediamine, and benzimidazole were purchased from Alfa Aesar. 4-Methoxy-nitrobenzene and 4-methoxy-phenylamine were purchased from Aladdin. Cetyltrimethylammonium bromide (CTAB) was obtained from Huishi Biochemical Reagent Company of China. Ammonia solution (27 wt %), ethanol and methanol were purchased from Beijing Chemical Works. Deionized water was used in all experiments. All reagents were used without further purification.

Synthesis of megranate-like nanoparticles

Yolk-shell nanoparticles[43] and megranate-like nanoparticles[21] were prepared according to literatures with some minor modifications. For the yolk-shell nanoparticles, the detailed synthesis procedures were provided in the supporting information. The yolk-shell nanoparticles were called silica nanorattles-SH and silica nanorattles-SO_3H. Megranate-like nanoparticles were prepared according to the following procedure: silica nanorattles-SH were impregnated with an aqueous solution of K_2PdCl_4, $HAuCl_4$, H_2PtCl_6 solution (10 g/L, 6 mL), then sonicated for 10 min in an ultrasonic bath, heated in an oven at 180 °C for 2 h under air environment. The dried particles were washed with water for several times. Finally, the resulting particles were collected by centrifugation and dried at ambient temperature. The megranate-like nanoparticles were called Pd-silica nanorattles-SH and Pd-silica nanorattles-SO_3H

Reduction of 4-methoxy-nitrobenzene using Pd cores in megranate-like nanoparticles

50 mg of megranate-like nanoparticles was homogeneously dispersed in 25 mL of methanol, followed by the addition 76 mg (0.5 mmol) of 4-methoxy-nitrobenzene, and the mixture was ultrasonicated for 10 min at room temperature. Then, the glass pressure vessel was charged with H_2 to 20 bar reacting for 12 h.[44] After reaction, the reaction mixture was diluted with methanol and the catalyst was separated by centrifugation.

Acid-catalyzed deprotection of benzaldehyde dimethyl acetal using silica nanorattles-SO_3H

Benzaldehyde dimethyl acetal (76 mg, 0.5 mmol) and water (41 mg, 2.3 mmol) were mixed in 5 mL of toluene at room temperature, followed by the addition of 10 mg of silica nanorattles-SH or silica nanorattles-SO_3H.[33] The resulting mixture was then stirred at reflux temperature for appropriate time. After reaction, the catalyst was separated by centrifugation.

Synthesis of the 2-(2-amidophenyl)-1H-benzimidazole using Pd-silica nanorattles-SO_3H catalyst

100 mg of bifunctional megranate-like nanoparticles was dispersed in 15 mL of methanol, followed by the addition of 66 mg (0.4 mmol) of 2-nitrobenzaldehyde and 54 mg (0.5 mmol) of 1, 2-phenylenediamine. The resulting mixture was stirred at reflux temperature under air atmosphere for 5 h and then transferred into a glass pressure vessel without any separation. The vessel was then charged with H_2 to 20 bar reacting for 8 h.[33] After reaction, the reaction mixture was diluted with methanol and the catalyst was separated by centrifugation.

Characterisation

TEM images and element mappings were obtained on FEI Tecnai G2 F20 s-twin D573 field emission transmission electron microscope with an accelerating voltage of 200 kV. SEM images were obtained on a JEOL JSM-6700F field-emission scanning electron microscope. The particle size was measured by photon correlation spectroscopy employing a Nano ZS90 laser particle analyzer (Malvern Instruments, UK) at 25 °C. N_2 adsorption-desorption isotherms were obtained at -196 °C on a Micromeritics ASAP 2420 surface area analyzer. Samples were degassed at 150 °C for a minimum of 12 h prior to analysis. Brunauer–Emmett-Teller (BET) surface areas were calculated from the linear part of the BET plot. The thermogravimetric analysis (TGA) curve was obtained in a flow of air from 35 to 800 °C (10 °C/ min) using a Netzsch STA 449C thermogravimetric analyzer. Powder XRD patterns were obtained by using a Rigaku 2550 diffractometer with Cu Kα radiation (λ=1.5418 Å). The adsorption of ammonia over the products was characterized by temperature-programmed desorption (NH_3-TPD, Micromeritics AUTOCHEM II 2920). The mass spectra were recorded in positive-ion mode on a Bruker-Esquire HCT instrument interfaced by an electrospray ionization source. High-performance liquid chromatograms (HPLC) were performed using the UltiMateTM 3000 system, including autosampler ASI-100, degasser DG-1210, pump P680 and Detector VWD-3400. The column was Acclaim TM 120, C18 (4.6×100 mm), 5 m. The mobile phase was the mixed solution of methanol and water with the volume ratio of 8: 2 and the flow-rate was 0.8 ml/min. The sample was injected with 9 µl every time detected by UV absorbance at 254 nm.

Results and discussion

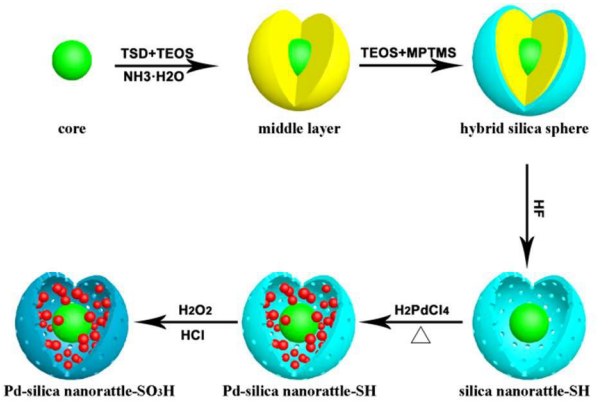

Scheme 1 Schematics for the synthesis of silica nanorattles-SH and the encapsulation of metal nanoparticles in silica nanorattles-SH

The whole synthetic pathway is shown in Scheme 1. Hybrid silica sphere consists of the core, the middle layer and the shell. Fig. 1a and Fig. 1b show representative scanning electron microscopy (SEM) and transmission electron microscopy (TEM) images of the hybrid silica spheres with a diameter about 500 nm. The images also show that the spheres are significantly monodisperse, smooth and uniform. To further confirm the uniform of the hybrid silica spheres, the hydrodynamic diameters of the samples are characterized by using dynamic light scattering (DLS). The observed hydrodynamic diameters are just slightly larger than those observed in the corresponding TEM images. This is understandable because hydrodynamic diameters are generally larger than the particle sizes observed by TEM.[45] Fig. 2a shows that average particle size changes from core (345 nm), middle layer (580 nm), to hybrid silica sphere (663 nm), respectively. After etching hybrid silica spheres with aqueous hydrofluoric acid (HF), we get silica nanorattles-SH. The SEM image (Fig. 1c) and TEM image (Fig. 1e) show that the silica nanorattles-SH are yolk-shell structure. Fig. 2a shows that the diameters of silica nanorattles-SH have partly shrank comparing with hybrid silica spheres. SEM image (Fig. 1d) is a broken sphere. It proves the existence of hollow structure between core and shell. Fig. 1f and Fig. 1g show high-resolution transmission electron microscopy (HRTEM) images of a silica nanorattle-SH, it confirms the existence of mesopores in the shell. We use nitrogen adsorption/desorption method to further prove the mesoporous structure of the silica nanorattles-SH (Fig. 2b). The hybrid silica spheres show only external surfaces. After adding an appropriate amount of aqueous hydrofluoric acid (HF), an increase in the surface area is observed for silica nanorattles-SH. The nitrogen absorption-desorption results demonstrate that the silica nanorattles-SH possess typical mesoporous structure. Fig. S1 shows the pore size distribution of the silica nanorattles-SH calculating from the adsorption branch of the nitrogen isotherm with the Barrett-Joyner-Halenda (BJH) method, which shows that the silica nanorattles-SH contain mesopores. The result confirms the mesoporous conclusion from TEM images. After immersion of silica nanorattles-SH in an aqueous solution of the given metal salt solution, we get megranate-like nanoparticles, here the silica nanorattles-SH act as a nanoreactor

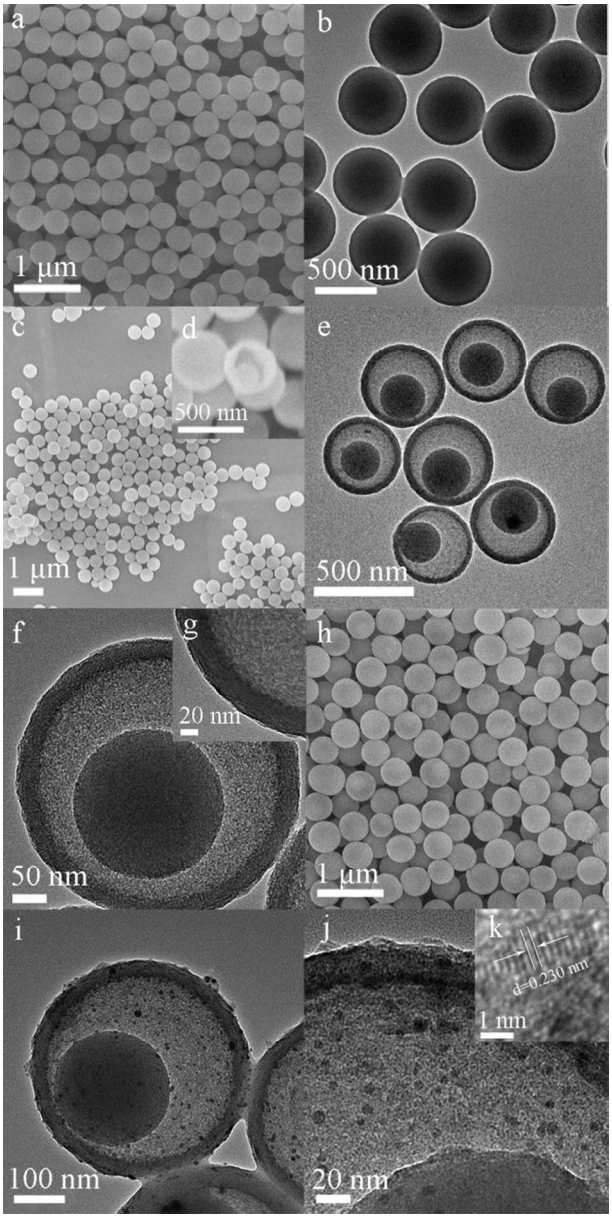

Fig. 1 a, b) SEM and TEM images of the hybrid silica spheres with diameter of 500nm (±10 nm) c, e) SEM and TEM images of silica nanorattles-SH (460nm±10 nm) d) SEM image showing a broken silica nanorattle-SH f, g) HRTEM image of a silica nanorattle-SH h) SEM image of the megranate-like Pd-silica nanorattles-SH i) TEM image and j, k) HRTEM images of megranate-like Pd-silica nanorattles-SH

and SH groups coordinate some metal nanoparticles.[46]

For megranate-like Pd-silica nanorattles-SH, SEM and TEM images (Fig. 1h, i) show that the Pd nanoparticles are mostly located inside the yolk-shell colloidal particles. Fig. 2a also shows the sizes of megranate-like Pd-silica nanorattles-SH shrink comparing with the silica nanorattles-SH. The main reason is the condensation of silica nanorattles-SH upon heating. Furthermore, the dispersivity and yolk-shell architecture of the silica nanorattles-SH are not affected after encapsulation of the metal salt solution. Fig. 2b shows a decrease in the surface area

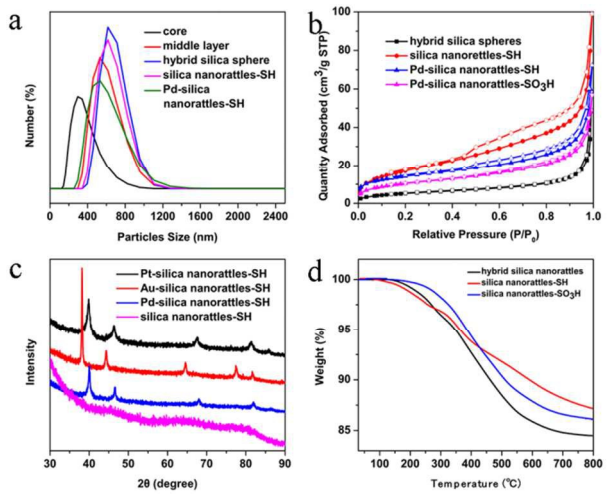

Fig. 2 a) Hydrodynamic diameters of core, middle layer, hybrid silica sphere, silica nanorattles-SH and megranate-like Pd-silica nanorattles-SH b) Nitrogen adsorption/desorption isotherms of hybrid silica spheres, silica nanorattles-SH, megranate-like Pd-silica nanorattles-SH and Pd-silica nanorattles-SO_3H c) The wide-angle XRD pattern of the different metal nanoparticles d) TG curves of hybrid silica spheres, silica nanorattles-SH and silica nanorattles-SO_3H

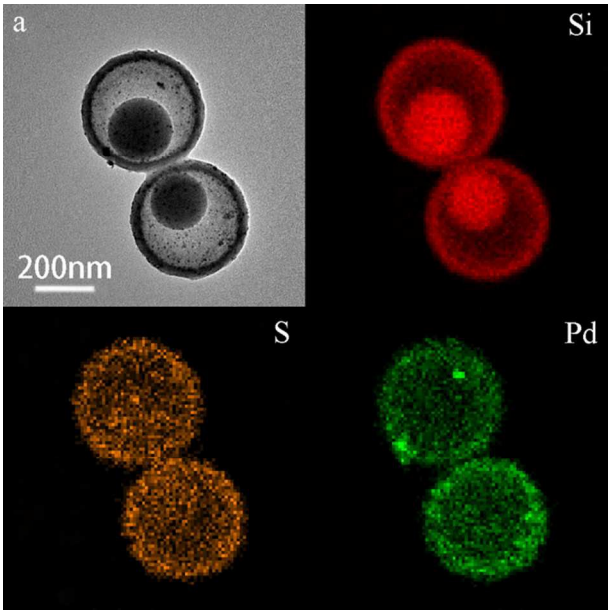

Fig. 3 Elemental mappings of megranate-like Pd-silica nanorattles-SH

for megranate-like Pd-silica nanorattles-SH and Pd-silica nanorattles-SO_3H, comparing with the silica nanorattles-SH, because Pd nanoparticles enter void space and shell of megranate-like nanoparticles. The HRTEM (Fig. 1j, k) images show that the metal nanoparticles are in the yolk-shell structures. The metal nanoparticles are visualized as dark dots. The lattice fringes are clearly visible, which can be attributed to the (111) planes of palladium.[47] The wide-angle XRD patterns (Fig. 2c) also indicate the presence of crystalline metal (Pd, Pt, Au) nanoparticles in silica nanoparticles-SH. From the XRD patterns, four metal diffraction peaks can be seen in the 2θ range 30-90°, assigning to (111), (200), (220), and (311) reflections of the cubic (fcc) metal nanoparticles lattice respectively. The X-ray photoelectron spectroscopy (XPS) result of sample Pd-silica nanorattles-SO3H is shown in Fig. S2. The Pd 3d XPS of the catalyst presents a doublet corresponding to Pd $3d_{5/2}$ and Pd $3d_{3/2}$. The Pd $3d_{5/2}$ peak at 335.3 eV is attributed to Pd^0 (metallic palladium), while the Pd $3d_{5/2}$ peak at 337.3 eV is related to Pd^{2+} (palladium oxide).[48, 49] According to XPS data, Pd^0 is formed as the major phase on the surface of the catalyst (~65%). The TEM and HRTEM images of megranate-like Pt-silica nanorattles-SH and Au-silica nanorattles-SH are provided in the Supporting Information (Fig. S3a, c, e and Fig. S3b, d, f). Fig. 2d shows thermo-behaviors of organic groups NH_2, SH, SO_3H in the hybrid silica spheres, silica nanorattles-SH and silica nanorattles-SO_3H. They show weight loss from 170 to 800 °C due to the decomposition of organic groups NH_2, SH, SO_3H and silica upon calcination.

TEM image and chemical mappings show the location of functional groups (-SH) in megranate-like Pd-silica nanorattles-SH. Fig. 3a is the TEM image of megranate-like Pd-silica nanorattles-SH. TEM image and elemental mappings results demonstrate the surface of the inner core, the void space, the inner and outer surface of shell in silica nanorattles-SH are all rich with Pd, and SH groups are mainly located on the shell (Fig. 3). The elemental mappings images also confirm that Pd nanoparticles of different sizes coexist inside the silica nanorattles-SH. The shell is rich with a very narrow size distribution of Pd nanoparticles, it is known that SH groups can coordinate Pd nanoparticles,[46] so most of the Pd nanoparticles locate in the surface of the shell. Some of the Pd nanoparticles locate in the hollow space. The big Pd nanoparticles may be formed by reuniting of adjacent small Pd nanoparticles during synthesis.[25] The other elemental mappings images of the megranate-like Pt-silica nanorattles-SH and Au-silica nanorattles-SH (Fig. S4, Fig. S5) are provided in the Supporting Information. They are similarly to Pd nanoparticles, small (Pt, Au) nanoparticles and large aggregated (Pt, Au) nanoparticles all can be seen.

The hydrogenation reaction of 4-methoxy-nitrobenzene to 4-methoxy-phenylamine[44] (Fig. 4a) is chosen as a model reaction to evaluate the catalytic activities and recyclability of the megranate-like Pd-silica nanorattles-SH. After the first catalysis, nearly 100% conversion of the reactant 4-methoxy-nitrobenzene and 98% yield of the desired product 4-methoxy-phenylamine are obtained. The

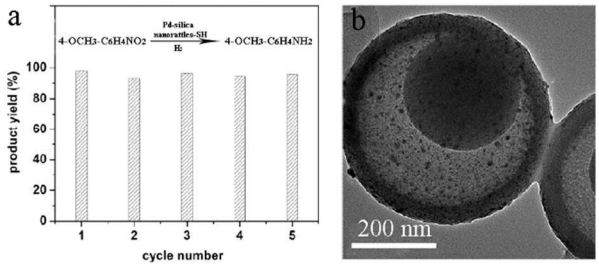

Fig. 4 a) Hydrogenation reaction of 4-methoxy-nitrobenzene to 4-methoxy-phenylamine and bar diagram for recycle ability of megranate-like Pd-silica nanorattles-SH in the hydrogenation reaction b) TEM image of megranate-like Pd-silica nanorattles-SH after the five cycles

megranate-like Pd-silica nanorattles-SH is efficiently recycled five times for the hydrogenation of 1-methoxy-4-nitro-benzene to 4-methoxy-phenylamine. Fig. 4a is bar diagram of five cycles, it shows that there is no obvious change in the activity even after five cycles. The TEM image of the final catalysts indicates that the nanostructure and dispersivity of the palladium nanoparticles have not changed after cycle reactions (Fig. 4b).

Silica nanorattles-SO_3H are facilely obtained through post-treatment of silica nanorattles-SH by oxidizing of the SH to SO_3H groups using H_2O_2.[46, 50, 51] The chemical mappings of silica nanorattles-SO_3H are also displayed in Fig. 5a. The chemical mappings show that the elements Si and O are evenly distributed within the spheres, the element S is mainly distributed on the shell. The acidic strength of silica nanorattles-SO_3H is experimentally investigated by temperature-programmed ammonia desorption (NH_3-TPD). Fig. 5b is the temperature programmed desorption (TPD) of NH_3 patterns. For the silica nanorattles-SH, small intense but broad NH_3 desorption signal is seen in this pattern. For the silica nanorattles-SO_3H before subjecting to the NH_3 adsorption, it shows small intense signal. These signals may be due to the decomposition/desorption of SO_3H groups.[52] For silica nanorattles-SO_3H, the total number of acidic sites is found to be much higher than silica nanorattles-SH and silica nanorattles-SO_3H before subjecting to the NH_3 adsorption. To validate the catalytic activity of silica nanorattles-SH and silica nanorattles-SO_3H, the acid-catalytic deprotection reaction of benzaldehyde dimethyl acetal to benzaldehyde is chosen as a probe reaction (Fig. 5c). The deprotection reaction will not proceed without acidic catalysts. When silica nanorattles-SH are used as the acidic catalysts, nearly 0% of the benzaldehyde dimethyl acetal is converted into benzaldehyde after reaction. In contrast, when the same dosage of silica nanorattles-SO_3H is used as the catalysts, nearly 100% of the benzaldehyde dimethyl acetal is converted into benzaldehyde. The higher acid-catalytic activity of silica nanorattles-SO_3H is attributed to the better acidity of silica nanorattles-SO_3H over silica nanorattles-SH. On the basis of these results, silica nanorattles-SO_3H obtained in this work are promising candidates for acidic catalysts.

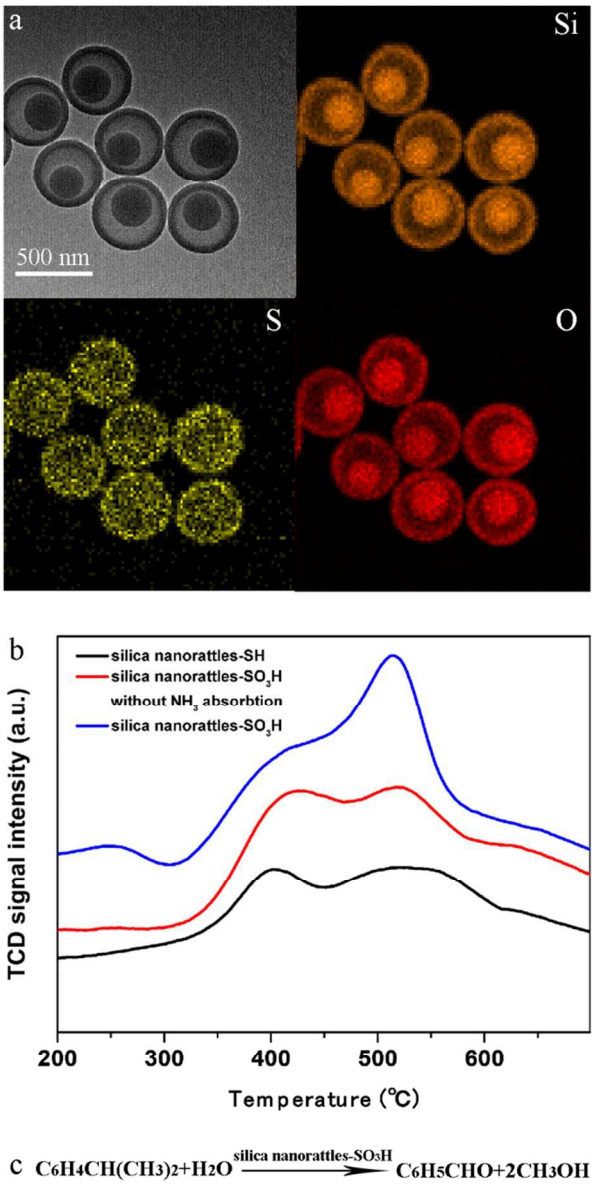

Fig. 5 a) Elemental mappings of silica nanorattles-SH b) Temperature programmed desorption (TPD) of NH_3 of silica nanorattles-SH after NH_3 adsorption; silica nanorattles-SO_3H without NH_3 adsorption and silica nanorattles-SO_3H (after NH_3 adsorption) c) reaction sequence of acid-catalytic deprotection of benzaldehyde dimethyl acetal to benzaldehyde

To demonstrate that the megranate-like Pd-silica nanorattles-SO_3H in this work own bifunctional properties, and can be used as catalysts for the multistep reaction involving an acidic catalysis and catalytic hydrogenation, the synthesis of benzimidazole derivatives is chosen as a model reaction (Fig. 6a).[33, 34] The as-synthesized megranate-like Pd-silica nanorattles-SO_3H are used as the catalysts for the synthesis of 2-(2-aminophenyl)-1H-benzimidazole from 2-nitrobenzaldehyde and 1,2-phenylenediamine. The reaction route is depicted in Fig. S6. The reactants (1, 2-phenylenediamine and 2-nitrobenzaldehyde) diffuse through the mesoporous SiO_2 shell, and conversion into 2-(2-nitrophenyl)-1H-benzimidazole is catalyzed by -SO_3H groups on the shell. The intermediate 2-(2-nitrophenyl)-1H-benzimidazole diffuses further and is converted into the final product, 2-(2-aminophenyl)-1H-benzimidazole; this reaction is catalyzed by the Pd nanoparticles located in the silica nanorattles-SO_3H. The intermediate 2-(2-nitrophenyl)-1H-benzimidazole is identified by mass spectrometry and ^{1}H NMR in the Supporting Information. After both acidic catalysis and hydrogenation steps, nearly 100% conversion of the reactant 2-nitrobenzaldehyde and 97% yield of the desired product 2-(2-aminophenyl)-1H-benzimidazole are obtained. In a control experiment, in the absence of Pd components in the catalysts, although silica nanorattles-SO_3H could catalyse the first step of the cascade reaction, it cannot give the conversion of the reactant into the final product 2-(2-aminophenyl)-1H-benzimidazole. The intermediate 2-(2-nitrophenyl)-1H-benzimidazole is obtained as the main product. The catalyst megranate-like Pd-silica nanorattles-SO_3H is efficiently recycled five times for the synthesis of 2-(2-

a

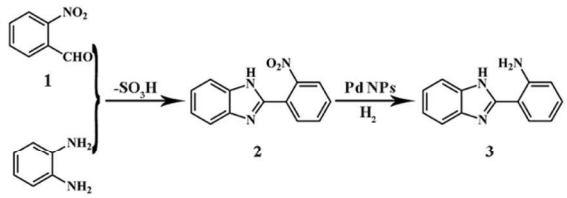

b

Cycle number	Con. of 1 (%)	Con. of 2 (%)	Yield. of 3 (%)	TOF (h^{-1})
1	100	100	97	6.2
2	100	100	90	5.6
3	100	100	88	5.5
4	100	100	87	5.4
5	100	100	86	5.4

Fig. 6 a) Multistep reaction sequence for the synthesis of 2-(2-aminophenyl)-1H-benzimidazole b) Table for recycle ability of megranate-like Pd-silica nanorattles-SO_3H in the cascade reaction, TOF is calculated by moles of product per molar Pd per hour

aminophenyl)-1H-benzimidazole and we also calculated the turnover frequency (TOF), which have been shown by the table in Fig. 6b and suggests that there is no obvious change in the activity even after five cycles. The high catalytic activity of the megranate-like Pd-silica nanorattles-SO_3H is due to two independent groups in one nanoreactor, which can shorten the reaction pathway. The masoporous SiO_2 shell allows fast diffusion of reactants and products, and protects the active Pd cores stable even under harsh conditions. The high catalytic performance confirms that the designed localization of Pd and SO_3H functionalities in megranate-like Pd-silica nanorattles-SO_3H indeed to be an effective catalyst for cascade reaction of synthesizing benzimidazole derivatives.

Conclusions

In conclusion, using simple yolk-shell nanoparticles as substrates, multifunctional megranate-like nanoparticles including multiple cores and SiO_2 shell have been synthesized. The cores can be different metal nanoparticles (Pd, Pt and Au) and the shell can be oxidized to acidic SO_3H groups. The whole megranate-like nanomaterials combine the properties of each component, and show good catalytic performance and recyclability in a cascade catalytic reaction of synthesizing benzimidazole derivatives. Silica nanorattles-SO_3H show high conversion (~100%) in the deprotection of benzaldehyde dimethyl acetal reaction. And Pd-silica nanorattles-SH show good catalytic activities in the reduction reaction of 4-methoxy-nitrobenzene to 4-methoxy-phenylamine.

Acknowledgements

This work was supported by the National Natural Science Foundation of China (Grant Nos. 21171064, 21371067 and 21373095).

Notes and references

State Key Laboratory of Inorganic Synthesis and Preparative Chemistry, College of Chemistry, Jilin University, Changchun 130012, China. E-mail: huoqisheng@jlu.edu.cn; Fax: +86-431-85168602; Tel: +86-431-85168602

Electronic Supplementary Material: Supplementary material (Figures show the TEM images, elemental mappings, NMR and HRMS results of the resultant samples)

1. J. Liu, S. Z. Qiao, J. S. Chen, X. W. Lou, X. Xing and G. Q. Lu, *Chem. Commun.*, 2011, **47**, 12578-12591.
2. X. Huang, M. G. Willinger, H. Fan, Z. L. Xie, L. Wang, A. K. Hoffmann, F. Girgsdies, C. S. Lee and X. M. Meng, *Nanoscale*, 2014, **6**, 8787-8795.
3. Z. Y. Wang, L. Zhou and X. W. Lou, *Adv. Mater.*, 2012, **24**, 1903-1911.
4. Y. Zhao and L. Jiang, *Adv. Mater.*, 2009, 21, 3621-3638.
5. R. B. Wu, X. K. Qian, K. Zhou, J. Wei, J. Lou and P. M. Ajayan, *ACS nano*, 2014, **8**, 6297-6303.
6. X. Fang, X. Zhao, W. Fang, C. Chen and N. F. Zheng, *Nanoscale*, 2013, **5**, 2205-2218.
7. H. Joshi, K. N. Sharma, A. K. Sharma and A. K. Singh, *Nanoscale*, 2014, **6**, 4588-4597.
8. C. B. Gao, Q. Zhang, Z. D. Lu and Y. D. Yin, *J. Am. Chem. Soc.*, 2011, **133**, 19706-19709.
9. J. G. Lee, J. C. Park and H. J. Song, *Adv. Mater.*, 2008, **20**, 1523-1528.
10. H. Hou, X. Cao, Y. Yang, L. Fang, C. Pan, X. Yang, W. Song and X. Ji, *Chem. Commun.*, 2014, **50**, 8201-8203.
11. J. C. Park and H. Song, *Nano Research*, 2011, **4**, 33-49.
12. A. Cao, R. Lu and G. Veser, *Phys. Chem. Chem. Phys.*, 2010, **12**, 13499-13510.
13. B. Liu, Q. Wang, S. Yu, P. Jing, L. Liu, G. Xu and J. Zhang, *Nanoscale*, 2014, **6**, 11887-11897.
14. J. Liu, S. Z. Qiao, Q. H. Hu and G. Q. Lu, *Small*, 2011, **7**, 425-443.
15. X. B. Li, Y. Yang and Q. H. Yang, *J. Mater. Chem. A.*, 2013, **1**, 1525-1535.
16. C. Li, H. Zhang, D. Jiang and Q. H. Yang, *Chem. Commun.*, 2007, 547-558.
17. L. Dong, S. Liu, H. Gao, N. Ding, W. Tremel, C. Xiong, Q. Zhu and W. Knoll, *Small*, 2009, **5**, 1153-1157.
18. Y. Wang, C. Ye, L. Wu and Y. Hu, *J. Pharm. Biomed. Anal.*, 2010, **53**, 235-242.
19. X. Wang, D. Liu, S. Song and H. Zhang, *J. Am. Chem. Soc.*, 2013, **135**, 15864-15872.
20. C. V. Luciani and K. Y. Choi, *Macromol. Theory Simul.*, 2014, **23**, 110-124.
21. J. Liu, H. Q. Yang, F. Kleitz, Z. G. Chen, T. Y. Yang, E. Strounina, G. Q. Lu and S. Z. Qiao, *Adv. Funct. Mater.*, 2012, **22**, 591-599.
22. Y. Wei, Z. Zhao, J. Liu, C. Xu, G. Jiang and A. Duan, *Small*, 2013, **9**, 3957-3963.
23. Z. W. Zhang, Y. M. Zhou, Y. W. Zhang, S. M. Xiang, S. J. Zhou and X. L. Sheng, *RSC Adv.*, 2014, **4**, 7313-7320.
24. J. Chen, Z. Xue, S. Feng, B. Tu and D. Zhao, *J. Colloid Interf. Sci.*, 2014, **429**, 62-67.
25. X. W. Lou, C. L. Yuan, E. Rhoades, Q. Zhang and L. A. Archer, *Adv. Funct. Mater.*, 2006, **16**, 1679-1684.
26. L. Li, D. Qin, X. Yang and G. Liu, *Polymer Chemistry*, 2010, **1**, 289-295.
27. G. L. Li and X. L. Yang, *J. Phys. Chem. B*, 2007, **111**, 12781-12786.
28. Y. S. Li and J. L. Shi, *Adv. Mater.*, 2014, **26**, 3176-3205.
29. R. Liu, Y. W. Yeh, V. H. Tam, F. Qu, N. Yao and R. D. Priestley, *Chem. Commun.*, 2014, **50**, 9056-9059.
30. C. Galeano, C. Baldizzone, H. Bongard, B. Spliethoff, C. Weidenthaler, J. C. Meier, K. J. J. Mayrhofer and F. Schüth, *Adv. Funct. Mater.*, 2014, **24**, 220-232.
31. B. Liu and H. C. Zeng, *Small*, 2005, **1**, 566-571.
32. E. C. Cho, P. H. Camargo and Y. N. Xia, *Adv. Mater.*, 2010, **22**, 744-748.
33. X. L. Fang, Z. H. Liu, M. F. Hsieh, M. Chen, P. X. Liu, C. Chen and N. F. Zheng, *ACS nano*, 2012, **6**, 4434-4444.
34. B. Guan, T. Wang, S. Zeng, X. Wang, D. An, D. Wang, Y. Cao, D. Ma, Y. Liu and Q. S. Huo, *Nano Research*, 2014, **7**, 246-262.

35. B. Liu, Q. Wang, S. Yu, T. Zhao, J. Han, P. Jing, W. Hu, L. Liu, J. Zhang, L. D. Sun and C. H. Yan, *Nanoscale*, 2013, **5**, 9747-9757.
36. P. M. Arnal, M. Comotti and F. Schuth, *Angew. Chem., Int. Ed.*, 2006, **45**, 8224-8227.
37. K. Dong, Z. Liu and J. S. Ren, *Cryst. Eng. Comm.*, 2013, **15**, 6329-6334.
38. L. Wang, J. Shi, Y. Zhu, Q. He, H. Xing, J. Zhou, F. Chen and Y. Chen, *Langmuir*, 2012, **28**, 4920-4925.
39. E. Merino, E. V. Sesto, E. M. Maya, M. Iglesias, F. l. Sánchez and A. Corma, *Chem. Mater.*, 2013, **25**, 981-988.
40. Q. Yang, J. Liu, L. Zhang and C. Li, *J. Mater. Chem.*, 2009, **19**, 1945-1955.
41. M. P. Lorenzo, B. Vaz, V. Salgueirino and M. A. C. Duarte, *Chem. Eur. J.*, 2013, **19**, 12196-12211.
42. M. Zhao, K. Deng, L. He, Y. Liu, G. Li, H. Zhao and Z. Tang, *J. Am. Chem. Soc.*, 2014, **136**, 1738-1741.
43. D. Chen, L. Li, F. Q. Tang and S. Qi, *Adv. Mater.*, 2009, **21**, 3804-3807.
44. M. A. Harrad, B. Boualy, L. E. Firdoussi, A. Mehdi, C. Santi, S. Giovagnoli, M. Nocchetti and M. A. Ali, *Catal. Commun.*, 2013, **32**, 92-100.
45. F. Lu, S. H. Wu, Y. Hung and C. Y. Mou, *Small*, 2009, **5**, 1408-1413.
46. Y. Yang, X. Liu, X. Li, J. Zhao, S. Bai, J. Liu and Q. H. Yang, *Angew. Chem., Int. Ed.*, 2012, **51**, 9164-9168.
47. B. Lim, M. Jiang, J. Tao, P. H. C. Camargo, Y. Zhu and Y. N. Xia, *Adv. Funct. Mater.*, 2009, **19**, 189-200.
48. Y. Wang, J. Yao, H. Li, D. Su and M. Antonietti, *J. Am. Chem. Soc.*, 2011, **133**, 2362-2365.
49. V. Z. Radkevich, T. L. Senko, K. Wilson, L. M. Grishenko, A. N. Zaderko and V. Y. Diyuk, *Appl. Catal. A*, 2008, **335**, 241-251.
50. J. Gao, J. Liu, S. Bai, P. Wang, H. Zhong, Q. Yang and C. Li, *J. Mater. Chem.*, 2009, **19**, 8580-8588.
51. Y. L. Huang, S. Xu and V. S. Y. Lin, *Angew. Chem., Int. Ed.*, 2011, **50**, 661-664.
52. S. Sreevardhan Reddy, B. David Raju, V. Siva Kumar, A. H. Padmasri, S. Narayanan and K. S. Rama Rao, *Catal. Commun.*, 2007, **8**, 261-266.